Controlled coalescence with local front reconstruction method

CONTROLLED COALESCENCE WITH LOCAL FRONT RECONSTRUCTION METHOD

A. H. RAJKOTWALA[1]*, H. MIRSANDI[1], E. A. J. F. PETERS[1], M. W. BALTUSSEN[1], C. W. M. VAN DER GELD [2], J. G. M. KUERTEN[3], J. A. M. KUIPERS[1]

[1]Multiphase Reactors Group, Department of Chemical Engineering and Chemistry, Eindhoven University of Technology, P.O. Box 513, 5600 MB Eindhoven, The Netherlands

[2]Process and Product Design Group, Department of Chemical Engineering and Chemistry, Eindhoven University of Technology, P.O. Box 513, 5600 MB Eindhoven, The Netherlands

[3]Multiphase and Reactive Flows Group, Department of Mechanical Engineering, Eindhoven University of Technology, P.O. Box 513, 5600 MB Eindhoven, The Netherlands

* E-mail: a.rajkotwala@tue.nl

ABSTRACT

The physics of droplet collisions involves a wide range of length scales. This poses a difficulty to accurately simulate such flows with traditional fixed grid methods due to their inability to resolve all scales with affordable number of computational grid cells. A solution is to couple a fixed grid method with simplified sub grid models that account for microscale effects. In this paper, we incorporate such framework in the Local Front Reconstruction Method (Shin *et al.*, 2011). To validate the new method, simulations of (near) head on collision of two equal tetradecane droplets are carried out at different Weber numbers corresponding to different collision regimes. The results show a better agreement with experimental data compared to other fixed grid methods like Front Tracking (Pan *et al.*, 2008) and Coupled Level Set and Volume of Fluid (CLSVOF) (Kwakkel *et al.*, 2013), especially at high impact velocities.

Keywords: Numerical Simulation, Multiphase flows, Front Tracking, LFRM, coalescence, break-up, droplet collision.

NOMENCLATURE

Greek Symbols

ρ	Mass density, $[kg/m^3]$.
μ	Dynamic viscosity, $[kg/ms]$.
σ	Surface tension coefficient, $[N/m]$.

Latin Symbols

p	Pressure, [Pa].
$\mathbf{u}$	Fluid Velocity, $[m/s]$.
$\mathbf{g}$	Gravitational acceleration, $[m/s^2]$.
$\mathbf{F}_\sigma$	Surface tension force, $[N/m^3]$.
t	time, [s].
$\mathbf{n}$	Surface normal.
t_c	Contact time between droplets, [s].
t_d	Film drainage time, [s].
R_0	Initial droplet radius, [m].
V_0	Initial droplet speed, $[m/s]$.
b	Offset distance between droplets, [m].

Sub/superscripts

Γ	Interface.
l	Liquid.

INTRODUCTION

Droplet-laden flows play an important role in many industrial applications and natural processes (Crowe *et al.*, 1998). Some examples are spraying of fuel in combustion engines, spray drying of food products, liquid-liquid extraction, growth of rain droplets in clouds and pollution tracking. The interaction between droplets has a major influence on the dynamics of such flows, because of the coalescence and break-up that may occur upon collision. However, it is very difficult to accurately capture coalescence and break-up numerically because of the wide range of length scales involved. For example, the collision dynamics of droplets is influenced by the drainage of the thin gas film separating two colliding droplets (Mason *et al.*, 2012), causing bouncing of the droplets when the film is not drained during the collision event. Coalescence occurs when the gas film ruptures. The rupture is attributed to the van der Waals surface forces which become dominant at nanometer scale. It is not possible to capture all scales ranging from millimeter (droplet diameter) to nanometer (critical film thickness) using an affordable number of computational grid cells.

In our fixed grid method, the under resolved final stage of the film drainage process is accounted for by a sub-grid model. Few studies have been done previously using different fixed grid methods and sub-grid models (Kwakkel *et al.*, 2013, Mason *et al.*, 2012). The fixed grid methods for modeling multiphase flows can be divided into two types: front capturing and front tracking techniques (Tryggvason *et al.*, 2011). In front capturing methods, the interface is implicitly represented by a colour function. Common front capturing methods are Volume of Fluid (VOF) (van Sint Annaland *et al.*, 2005), Level Set (LS) (Sethian and Smereka, 2003) and Coupled Level Set and Volume of Fluid (CLSVOF) (van der Pijl *et al.*, 2005) methods. Generally, the droplets in these methods coalesce automatically when they share a common grid cell. However, this numerical coalescence can be avoided for the simulation of symmetric binary droplet collision using Volume of Fluid method. The coalescence can be controlled by prescribing a volume-fraction boundary condition on the collision plane using ghost cells (Mason *et al.*, 2012). When the boundary condition is set to zero volume fraction, the droplets will bounce; whereas a symmetry boundary condition will result in coalescence. A more general approach to avoid numerical coalescence is to use unique colour function for each droplet (Nikolopoulos *et al.*, 2009).

A big disadvantage of front capturing methods is the very fine grid resolution which is required for accurate surface

tension calculation especially when the droplets undergo complex topological changes (Kwakkel *et al.*, 2013). Front tracking methods (Dijkhuizen *et al.*, 2010, Shin *et al.*, 2011) are inherently better at surface tension calculation at coarse grid resolution. This is because a front tracking method directly tracks the interfaces using triangular marker elements, enabling accurate curvature calculation. However, in the traditional front tracking method, droplet coalescence is not possible. To incorporate coalescence, additional routines to merge the individual unstructured meshes belonging to different droplets are required (Nobari *et al.*, 1996). In the traditional front tracking method, the merging of the droplet meshes is complicated because the logical information about the marker connectivity should be updated. In addition, the merging of droplets with complex topology is very challenging. Therefore, we choose a front tracking method without connectivity, the Local Front Reconstruction Method (LFRM) by Shin *et al.*, 2011.

As logical connectivity between marker elements is not required, LFRM can handle complex topological changes like droplet coalescence and pinch off. It uses information from the original marker elements directly to reconstruct the interface in a mass conservative manner and thus, also ensures good local mass conservation. Because the interface is reconstructed independently in each individual reconstruction cell, the method can be highly parallelized. However, this cell-oriented reconstruction leads to numerical coalescence (similar to front capturing methods) in LFRM (Shin *et al.*, 2011). This is prevented in our implementation by storing the information about marker elements and marker points for each droplet separately. The coalescence is accomplished by merging data-structures of two droplets. Similarly, the break-up of a droplet is done by splitting the data-structure of the droplet. The details of these procedures are given in next section. We have improved the original LFRM method in certain areas which are also summarized in next section. Lastly, the results of simulations of (near) head on collision of two equal tetradecane droplets in different collision regimes are discussed. The discussion includes validation of simulations with experimental data and comparison with other fixed grid methods (Kwakkel *et al.*, 2013, Pan *et al.*, 2008).

METHODOLOGY

Local Front Reconstruction Method

Both fluids in the two phase flow are assumed to be incompressible, immiscible and Newtonian fluids. A one-fluid formulation is used and the governing equations are given by the continuity equations and the Navier-Stokes equations, where the physical properties depend on local phase fractions.

$$\nabla \cdot \mathbf{u} = 0 \tag{1}$$

$$\rho \frac{\partial \mathbf{u}}{\partial t} + \rho \nabla \cdot (\mathbf{u}\mathbf{u}) = -\nabla p + \rho \mathbf{g} + \nabla \cdot \mu \left[\nabla \mathbf{u} + (\nabla \mathbf{u})^T \right] + \mathbf{F}_\sigma \tag{2}$$

where $\mathbf{F}_\sigma$ is a singular source-term to represent the surface tension at the interface.

The following conditions are applied at the interface Γ to close the governing equations:

$$[\mathbf{u}]_\Gamma = 0 \tag{3}$$

$$\left[-p\mathbf{n} + \mu \left(\nabla \mathbf{u} + (\nabla \mathbf{u})^T \right) \cdot \mathbf{n} \right]_\Gamma = \mathbf{S}_\sigma \cdot \mathbf{n} \tag{4}$$

where $[.]_\Gamma$ represents jump in a quantity across the interface from one phase to another and $\mathbf{S}_\sigma$ is the surface force acting on interface due to surface tension.

The equations are discretized using a finite volume approach and are solved on a staggered computational grid by a fractional step method (Das *et al.*, 2017). The surface tension force $\mathbf{F}_\sigma$ is calculated using hybrid surface tension model (Shin *et al.*, 2005) which has combined advantage of accurate curvature calculation (similar to the pull force model which is commonly used in front tracking methods) and proper balance of pressure and surface tension force at discrete level (similar to the continuum surface model which is commonly used in front capturing methods).

The fluid velocity is interpolated from Eulerian grid to Lagrangian grid using cubic spline interpolation and marker points are moved with the interpolated velocity using a 4^{th} order Runge-Kutta scheme (Dijkhuizen *et al.*, 2010).

As mentioned before, the local phase fraction is required to calculate the averaged physical properties. This can be calculated by the geometric analysis using the positions of the marker points (Dijkhuizen *et al.*, 2010). This method of phase fraction calculation is exact and computationally more efficient than the traditional method of solving Poisson equation used in original LFRM method. From the calculated phase fractions, the average density and viscosity is calculated by algebraic and harmonic averaging, respectively.

Due to the advection of the marker points, the marker elements can become too large or too small. This poor grid quality decreases the accuracy of the surface tension force calculation. To maintain the mesh quality, a mesh reconstruction procedure of (Shin *et al.*, 2011) is implemented. The reconstruction procedure also allows to reconstruct the mesh when the multiple droplets coalesce or a droplet breaks-up. The implementation is improved by the use of linked-list data-structures for storing location of the three vertices of each marker. This ensures that each marker point has a unique identity, thus reducing the memory requirements and preventing precision problems.

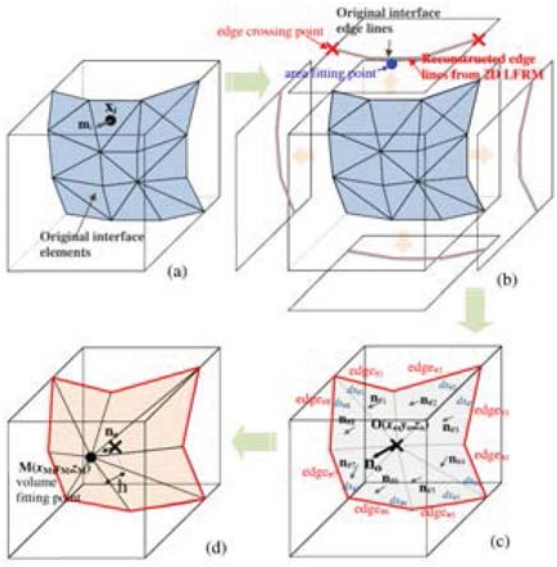

Figure 1: Schematic of the reconstruction procedure for LFRM (Shin *et al.*, 2011).

The overall reconstruction procedure consists of four simple steps as shown in Figure 1:

(a) Localization - Interface of the discrete phase is cut by a reconstruction grid (similar to the Eulerian grid) such that each part of the interface lies completely inside one cell.

(b) Edge line reconstruction - The edge line corresponding to the cut interface is traced out on relevant faces of the cell, and new edge line (containing only two edge points and a fitting point) is reconstructed in an area conservative manner.

(c) Centroid calculation - Using edge points and fitting points of all the faces, a centroid is calculated. An intermediate interface is formed by connecting the centroid with intermediate edge lines.

(d) Volume fitting - Finally, the centroid is moved in the normal direction of intermediate interface such that original volume of the dispersed phase is conserved in the given cell.

Flows involving coalescence and break-up of the dispersed phase are easily handled by LFRM. This is enabled by the marker reduction and the tetra-marching procedures, which allow merging and breaking of unstructured meshes of the dispersed phase. Details of these procedures can be found in (Shin *et al.*, 2011). In our implementation, the data-structure of each droplet is stored with a unique identity. However, this prevents coalescence completely. To enable coalescence between two droplets at a desired time, their data-structures have to be merged and the merged droplet has to be given a unique identifier, which is handled by the coalescence module. Similarly, each daughter droplet is given a unique identifier when formed after break-up of a droplet, which is handled by the break-up module.

Coalescence Module

The coalescence module checks if there are multiple interfaces within the same reconstruction cell and combines the data-structures of two droplets depending on the calculated film drainage and contact time. The different steps in the coalescence module are given below:

(a) Bounding box for droplets in terms of grid cell units is calculated (Figure 2(a)).

(b) At each time step, it is checked if the bounding boxes of any two droplets are overlapping.

(c) If the overlap exists, the cells containing interfaces from both droplets are flagged to check if any cell contains interface from both droplets (Figure 2(b)).

(d) If one or more cells contain interface from both droplets, then these droplets are identified to be in 'contact' and added to a collision list (Figure 2(c)). The contact timer is initiated to keep track of contact time t_c.

(e) At each time step, it is checked if the droplets pair is still in contact. If a pair is in contact, the contact time is compared to the film drainage time t_d. In this study, the film drainage time t_d is obtained from experiments. If the contact exists and $t_c > t_d$, the data-stuctures of two droplets are merged and reconstruction is performed to execute droplet coalescence (Figure 2(e)). If the contact ceases, the droplets are removed from the collision list and this leads to bouncing of droplets.

Break-up Module

The numerical break-up of the droplet will take place based on the size of the reconstruction grid. As stated before, it is important to separate the data-structure of the droplets after break-up to avoid numerical coalescence. This separation is achieved by using a recursive flagging algorithm. The algorithm is used to find the disjoint droplets that are subsequently assigned a new 'droplet-number', see Figure 3.

RESULTS

In case of (near) head-on collisions between equal sized hydrocarbon droplets, four regimes of collision outcome are observed with increasing Weber number (measure of droplet inertia compared to surface tension). As seen in Figure 4, these regimes are (I) Coalescence with minor deformation, (II) Bouncing, (III) Coalescence with major deformation and (IV) Coalescence with separation resulting in production of daughter droplets. To validate the modified LFRM method, a

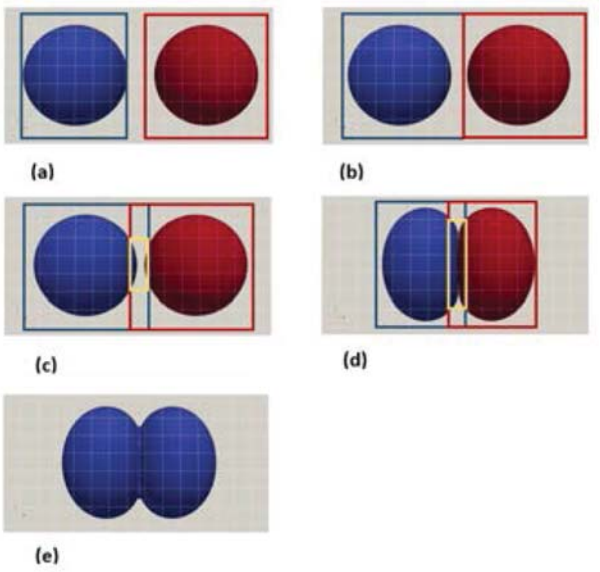

Figure 2: Schematic of the coalescence module. Blue and red boxes represent bounding boxes of blue and red droplets respectively. Yellow box represents cells containing interface from both droplets.

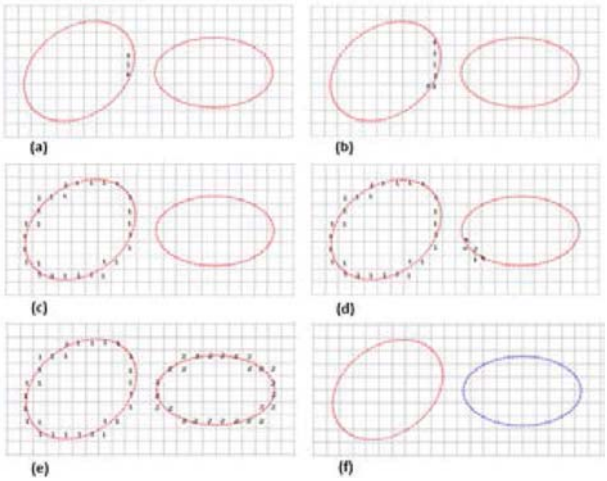

Figure 3: Steps of flagging algorithm in the break-up module.

case of binary droplet collision from each of these regimes is simulated and compared with experiments (Pan *et al.*, 2008 and Qian and Law, 1997) and other simulation methods (Pan *et al.*, 2008 and Kwakkel *et al.*, 2013).

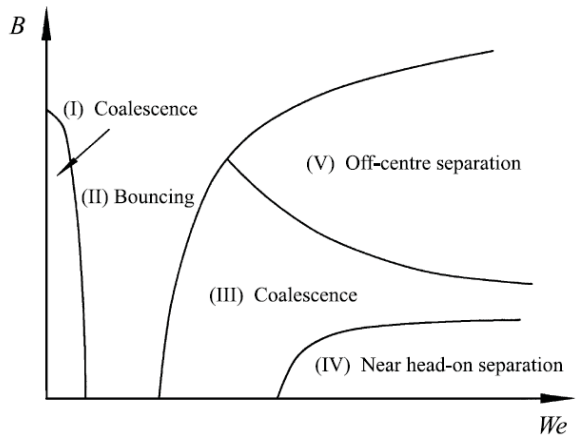

Figure 4: Schematic of collision regimes of two equal sized hydrocarbon droplets in atmospheric pressure. The parameter B represents the obliqueness of the collision and We represents the Weber number (Qian and Law, 1997).

The grid cell size is selected such that 12 grid cells are taken across the droplet radius (R_0) (similar to grid size used in (Kwakkel *et al.*, 2013) for CLSVOF and (Pan *et al.*, 2008) for FT). The computational domain has dimensions $8R_0 \times 10R_0 \times 8R_0$ with the largest dimension in the direction of the collision. Free slip boundary condition is used on all domain boundaries. The initial distance between the droplet centers is taken as $2.8R_0$. Each droplet is initialised with a uniform velocity field, V_0, but in the opposite direction. For each case, Weber number and impact parameter (Figure 5) are provided as an input. The film drainage time is provided by experimental observations (Pan *et al.*, 2008).

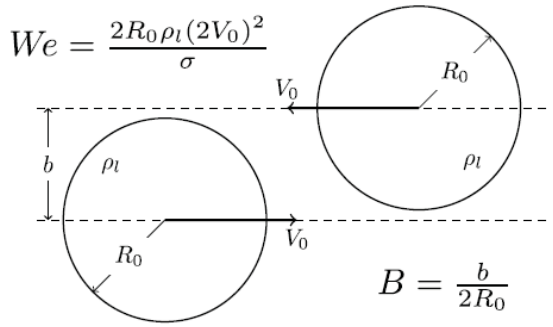

Figure 5: Nomenclature of general binary droplet collision (Kwakkel *et al.*, 2013).

Regime I

This regime always results in coalescence, while the collisions are gentle (low Weber numbers). A collision of tetradecane droplets in 1 atm. air, $R_0 = 107.2\,\mu$m , $V_0 = 0.305$ m/s, $We = 2.3$, and $B = 0$ is shown in Figure 6. The obtained result from LFRM matches well with results from the Coupled Level Set Volume of Fluid method (Kwakkel *et al.*, 2013), the Front Tracking method (Pan *et al.*, 2008) and experimental data (Pan *et al.*, 2008). In such regime, the coalescence happens around maximum deformation. After the coalescence, the cusp at the merged interface is quickly flattened. This phenomenon is nicely captured by all the numerical simulations.

Regime II

This regime always results in bouncing. A collision of tetradecane droplets in 1 atm. air, $R_0 = 167.6\,\mu$m, $V_0 = 0.492$ m/s, $We = 9.33$, and $B = 0$ is shown in Figure 7. Again, the results obtained using LFRM agree well with experimental data (Pan *et al.*, 2008) and other simulation results with FT (Pan *et al.*, 2008) and CLSVOF (Kwakkel *et al.*, 2013).

Regime III

This regime always results in coalescence, however the collisions are hard collision (high weber numbers) resulting in substantial deformation before merging. A collision of tetradecane droplets in 1 atm. air, $R_0 = 169.7\,\mu$m, $V_0 = 0.591$ m/s, $We = 13.63$, and $B = 0$ is shown in Figure 8. The merging in this case occurs as the deformed droplet is flattened to a disk shape while the incoming mass at the center of the rear face is still heading forward resulting in dimpled shape between 370 and 500 ms. Although this is not very clear in the experimental results (Pan *et al.*, 2008) but it was captured properly by all the numerical simulations.

Regime IV

This regime of near head on collision results in separation of droplets after merging as the kinetic energy is sufficient to overcome the surface energy. A collision of tetradecane droplets in 1 atm. nitrogen, $R_0 = 168\,\mu$m, $V_0 = 1.260$ m/s, $We = 62.2$, and $B = 0.06$ is shown in Figure 9. A zero film drainage time (which is justified by high weber number) is used in the simulation. The different colour of droplets indicate that each droplet has different droplet number and separate data-structure.

The results obtained using LFRM match better with the experimental results (Qian and Law, 1997) compared to the CLSVOF (Kwakkel *et al.*, 2013). In Figure 9, a premature separation is seen for CLSVOF. As explained in (Kwakkel *et al.*, 2013), the origin of this premature separation is the less accurate curvature estimation in strongly deformed regions. These errors in curvature estimation have a direct consequence for the acting surface tension force, and over time the droplet shape. This indicates that LFRM has more accurate surface tension calculation for the same grid size. Also, the size of the satellite droplet resembles the experimental data better compared to the CLSVOF results.

CONCLUSION

The local front reconstruction method has been improved and extended to allow for controlled coalescence. The new method has been successfully validated by carrying out simulations of binary (near) head on droplet collisions. By using experimentally observed film drainage times, a good match with experimental data is observed. This shows that if an accurate predictions of the film drainage time can be obtained from a sub-grid model, LFRM can capture collision dynamics in multiphase flows with physical realism. Finally, the results obtained using LFRM are compared with those of other methods and a better agreement with experimental data is seen, especially at high impact velocities.

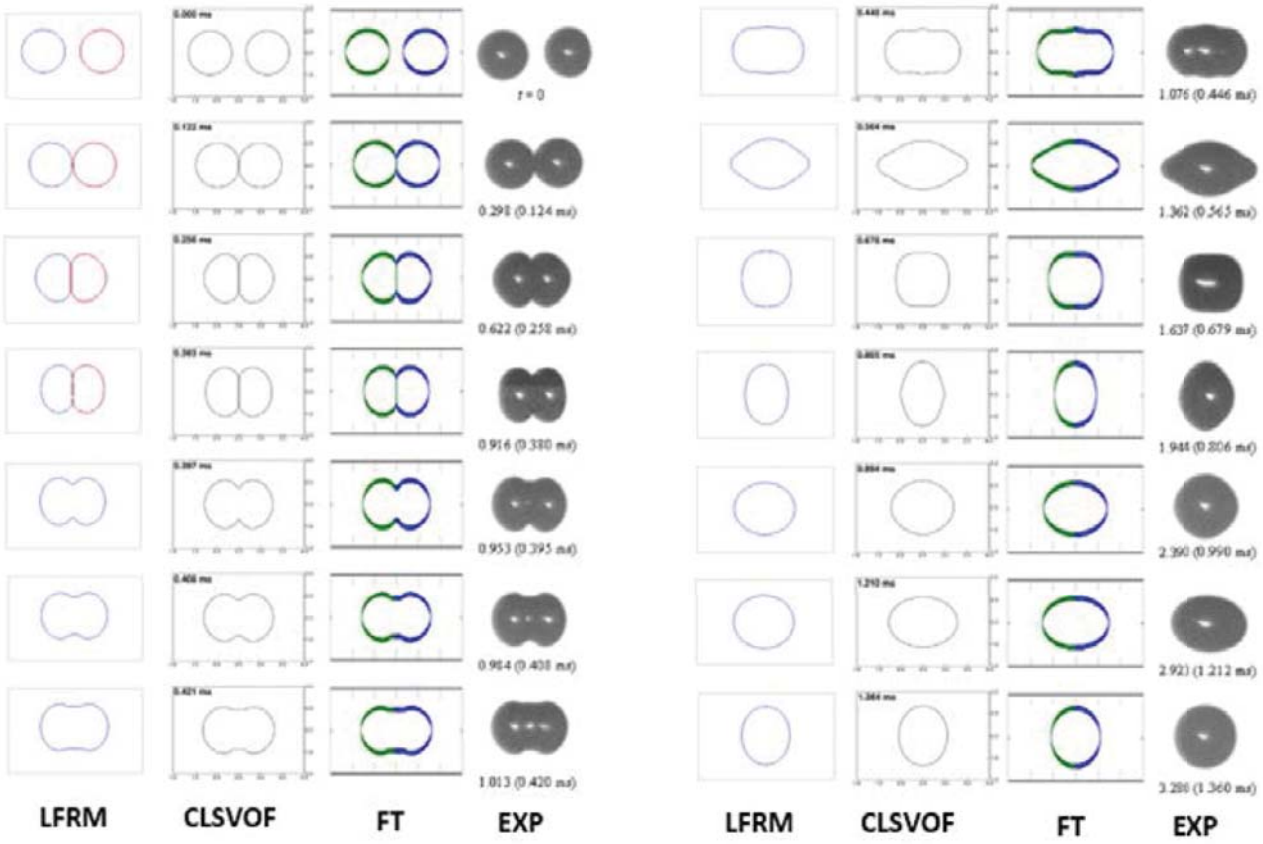

Figure 6: Merging collision sequence in regime I. LFRM results from present study, CLSVOF from (Kwakkel *et al.*, 2013), FT and experimental results from (Pan *et al.*, 2008). Conditions: tetradecane in 1 atm. air, $R_0 = 107.2\,\mu$m, $V_0 = 0.305$ m/s, $We = 2.3$, and $B = 0$. The film drainage time observed in experiments is $t_d = 0.270$ ms.

ACKNOWLEDGEMENT

This work is part of the research programme Open Technologieprogramma with project number 13781, which is (partly) financed by the Netherlands Organisation for Scientific Research (NWO) Domain Applied and Engineering Sciences (TTW, previously Technology Foundation STW).

REFERENCES

CROWE, C., SOMMERFELD, M. and TSUJI, Y. (1998). *Multiphase flows with droplets and particles*. CRC Press, Boca Raton.

DAS, S., DEEN, N.G. and KUIPERS, J.A.M. (2017). "Immersed boundary method (ibm) based direct numerical simulation of open-cell solid foams: Hydrodynamics". *AIChE Journal*, **63(3)**, 1152–1173.

DIJKHUIZEN, W., ROGHAIR, I., ANNALAND, M.V.S. and KUIPERS, J. (2010). "DNS of gas bubbles behaviour using an improved 3d front tracking model - model development". *Chemical Engineering Science*, **65(4)**, 1427 – 1437.

KWAKKEL, M., BREUGEM, W.P. and BOERSMA, B.J. (2013). "Extension of a CLSVOF method for droplet-laden flows with a coalescence/breakup model". *Journal of Computational Physics*, **253**, 166 – 188.

MASON, L., STEVENS, G. and HARVIE, D. (2012). "Multi-scale volume of fluid modelling of droplet coalescence". *Ninth International Conference on CFD in the Minerals and Process Industries*. CSIRO, Melbourne, Australia.

NIKOLOPOULOS, N., NIKAS, K.S. and BERGELES, G. (2009). "A numerical investigation of central binary collision of droplets". *Computers & Fluids*, **38(6)**, 1191 – 1202.

NOBARI, M.R., JAN, Y.J. and TRYGGVASON, G. (1996). "Headon collision of drops - a numerical investigation". *Physics of Fluids*, **8(1)**, 29–42.

PAN, K.L., LAW, C.K. and ZHOU, B. (2008). "Experimental and mechanistic description of merging and bouncing in head-on binary droplet collision". *Journal of Applied Physics*, **103(6)**, 064901.

QIAN, J. and LAW, C. (1997). "Regimes of coalescence and separation in droplet collision". *Journal of Fluid Mechanics*, **331**, 59–80.

SETHIAN, J.A. and SMEREKA, P. (2003). "Level set methods for fluid interfaces". *Annual Review of Fluid Mechanics*, **35(1)**, 341–372.

SHIN, S., ABDEL-KHALIK, S.I., DARU, V. and JURIC, D. (2005). "Accurate representation of surface tension using the level contour reconstruction method". *J. Comput. Phys.*, **203(2)**, 493–516.

SHIN, S., YOON, I. and JURIC, D. (2011). "The local front reconstruction method for direct simulation of two- and three-dimensional multiphase flows". *Journal of Computational Physics*, **230(17)**, 6605 – 6646.

TRYGGVASON, G., SCARDOVELLI, R. and ZALESKI, S. (2011). *Direct Numerical Simulations of Gas-Liquid Multiphase Flows*. Cambridge University Press, Cambridge.

VAN DER PIJL, S., SEGAL, A., VUIK, C. and WESSELING, P. (2005). "A mass-conserving Level-Set method for modelling of multi-phase flows". *International Journal for*

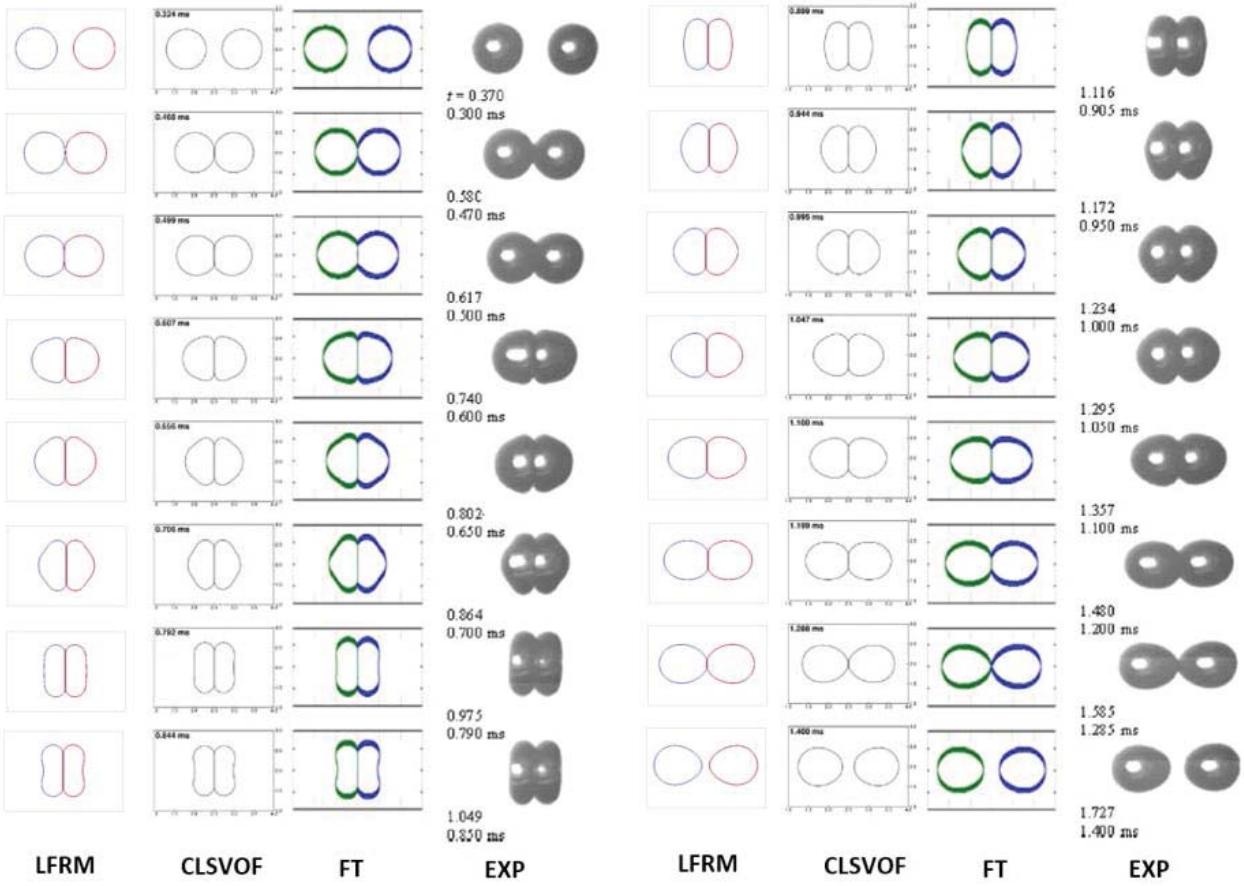

Figure 7: Bouncing collision sequence in regime II. LFRM results from present study, CLSVOF from (Kwakkel *et al.*, 2013), FT and experimental results from (Pan *et al.*, 2008). Conditions: tetradecane in 1 atm. air, $R_0 = 167.6\,\mu$m, $V_0 = 0.492$ m/s, $We = 9.33$, and $B = 0$.

Numerical Methods in Fluids, **47**, 339–361.

VAN SINT ANNALAND, M., DEEN, N. and KUIPERS, J. (2005). "Numerical simulation of gas bubbles behaviour using a three-dimensional volume of fluid method". *Chemical Engineering Science*, **60(11)**, 2999–3011.

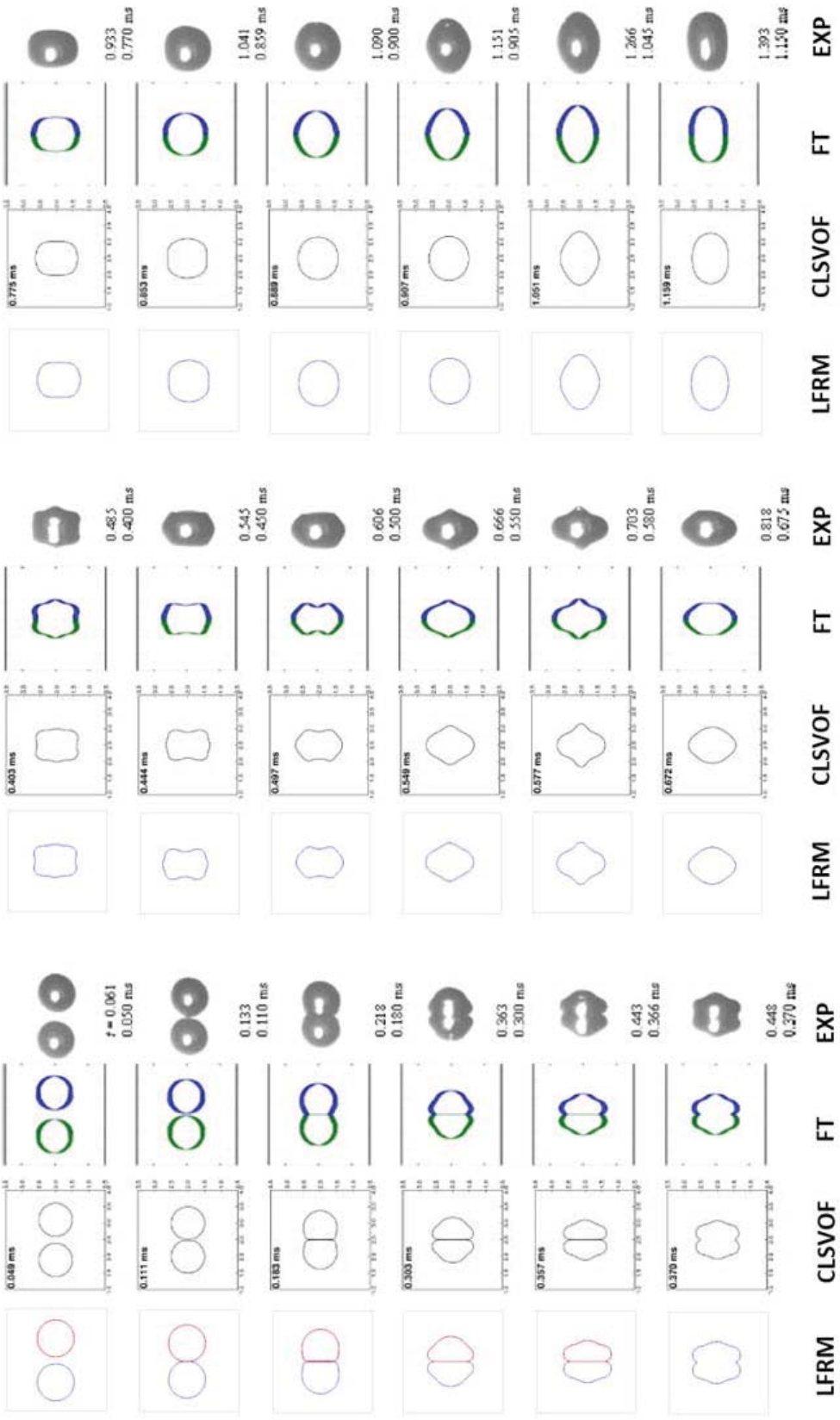

Figure 8: Merging collision sequence in regime III. LFRM results from present study, CLSVOF from (Kwakkel *et al.*, 2013), FT and experimental results from (Pan *et al.*, 2008). Conditions: tetradecane in 1 atm. air, $R_0 = 169.7\,\mu$m, $V_0 = 0.591$ m/s, $We = 13.63$, and $B = 0$. The film drainage time observed in experiments is $t_d = 0.246$ ms.

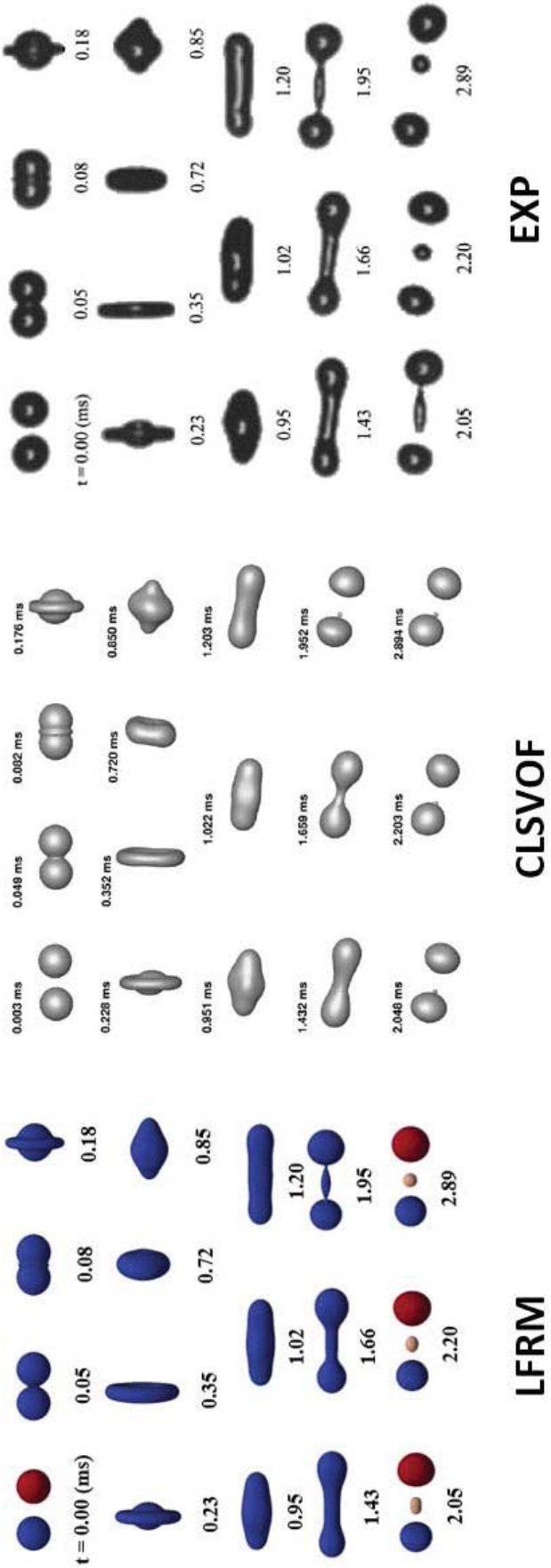

Figure 9: Near head on separating collision sequence in regime IV. LFRM results from present study, CLSVOF from (Kwakkel *et al.*, 2013) and experimental results from (Qian and Law, 1997). Conditions: tetradecane in 1 atm. nitrogen, $R_0 = 168\,\mu\text{m}$, $V_0 = 1.260$ m/s, $We = 62.2$, and $B = 0.06$. The film drainage time is assumed to be zero.